Semianalytical approach to the design of photonic crystal cavities

Marco Felici,* Kirill A. Atlasov, Alessandro Surrente, and Eli Kapon
Laboratory of Physics of Nanostructures, École Polytechnique Fédérale de Lausanne (EPFL), CH-1015 Lausanne, Switzerland
(Received 25 March 2010; revised manuscript received 14 June 2010; published 20 September 2010)

Most current methods for the engineering of photonic crystal (PhC) cavities rely on cumbersome, computationally demanding trial-and-error procedures. In the present work, we take a different approach to the problem of cavity design, by seeking to establish a direct, semianalytic relationship between the target electromagnetic field distribution and the dielectric constant of the PhC structure supporting it. We find that such a relationship can be derived by expanding the modes of L_N-type cavities as a linear combination of the one-dimensional (1D) Bloch eigenmodes of a PhC W1 waveguide. Thanks to this expansion, we can also ascertain the presence of a well-defined 1D character in the modes of relatively short cavities (e.g., L_{9-15}), thus confirming recent theoretical predictions and experimental findings. Finally, we test our method through the successful design of a cavity supporting a mode with Gaussian envelope function and ultralow radiative losses (quality factor of 17.5×10^6).

DOI: 10.1103/PhysRevB.82.115118 PACS number(s): 42.70.Qs, 78.20.Bh, 42.60.Da

I. INTRODUCTION

In semiconductor physics, the study of how the incorporation—either deliberate or unintentional—of defects and impurities affects the properties of a host material represents a subject of ever-growing importance. In some instances, the presence of these defects represents an unwanted nuisance; this is the case, for example, of surface recombination centers in semiconductor solar cells, lasers, and detectors.[1] On the other hand, the continuous development of epitaxial growth techniques has given rise to the possibility of incorporating controlled percentages of specific impurities in a semiconducting crystal, thus providing the freedom to tailor the optical, electrical, and structural properties of a grown sample on a monolayer-by-monolayer basis.[2] As a matter of fact, this great flexibility is probably the main reason behind the pervasive presence of semiconductors in modern-day electronic components.

Even though material systems based on the incorporation of *deep impurities* (such as nitrogen in III-V materials[3]) have recently shown some promise,[4–8] defects selected to alter the properties of semiconductors generally fall into the category of *shallow* impurities (e.g., donors and acceptors or conventional isoelectronic impurities). Probably, the property that best defines this class of impurities is represented by the relatively large spatial extension of their carrier wave functions (typically, many primitive cells of the crystal). Being highly delocalized in real space, these wave functions can be reconstructed from a few Bloch functions of the host crystal, having wave vector $\vec{k}$ nearly equal to that of the nearest band extremum.[9] This, in turn, allows for several simplifications, which ultimately result in the possibility of formulating semianalytical models that describe and predict the effects of the incorporation of shallow impurities in the host material. In the absence of such models (as, for example, in the case of most deep impurities), any attempt at adjusting the properties of semiconductors through the deliberate introduction of defects would have to rely on lengthy trial-and-error procedures.

Currently, such a trial-and-error approach dominates the practice of *defect engineering* in photonic crystals (PhCs). The possibility that a disruption of the periodicity of the photonic lattice might confine light,[10] much in the same way as defects and impurities trap carriers in a semiconducting crystal, was suggested immediately after the first proposal of PhCs.[11] In the last decade, a great number of experimental demonstrations of this concept have appeared in the literature, *en route* to the realization of PhC cavities[12] and waveguides,[13] PhC microcavity lasers,[14,15] and strongly coupled quantum dot (QD)-PhC cavity systems.[16–18] A vast majority of these experiments is based on PhC membrane L_N *cavities*,[19] which are obtained by simply removing a line of N air holes from a two-dimensional (2D) PhC hexagonal lattice [see Fig. 1(a)], embedded in a thin semiconductor slab (or membrane). The L_3 cavity, in particular, has enjoyed a widespread diffusion,[15–17,20] because of its capability to confine light in very small volumes (below one cubic wavelength) while also attaining high quality factors (Q).

In recent years, extensive efforts have been directed at the minimization of radiative losses in optimized L_3 cavities,[21,22] in an attempt to achieve Q factors that would allow for the observation of pronounced cavity quantum electrodynamics effects. Through a fine tuning of the arrangement of the holes near the cavity terminations, theoretical Q factors in excess of 10^5 could be obtained;[22] however, L_3-like cavities have proven rather difficult to optimize beyond this point, in spite of their conceptual simplicity and of a relative ease of fabrication. Generally speaking, it is relatively straightforward to identify two main origins for this problem. From a physical point of view, an intrinsic justification for the presence of significant radiative losses in short L_N-like cavities resides in the excessively abrupt variation in the mode's spatial distribution in proximity of the cavity terminations, as first suggested by Akahane *et al.* in Ref. 21. Eventually, this consideration led to the development of a new class of line-defect PhC cavities—whose dielectric constant distribution differs significantly from that of L_N cavities—in which light is "confined gently in order to be confined strongly"[21] and radiative losses are greatly suppressed (theoretical Q factors in excess of 10^7).[23] From a more practical standpoint, however, a

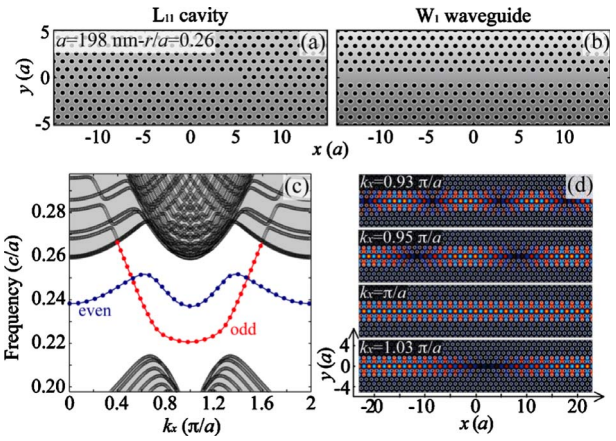

FIG. 1. (Color online) (a) Example of PhC membrane L_N cavity ($N=11$). The PhC parameters used in the computation of the cavity modes ($a=198$ nm, $r/a=0.26$) are indicated. The same parameters were used for the PhC W1 waveguide shown in (b). (c) Waveguide dispersion as obtained from 2DFD computations. The bands that are spatially confined in the waveguide are shown in gray (red) (*odd* modes) and black (blue) (*even* modes). (d) Real part of the E_y component of four eigenmodes belonging to the odd waveguide band shown in (c). The modes were randomly selected around the minimum of the band, in $k_x=\pi/a$. The corresponding k_x values are indicated.

second important reason for the difficulty of optimizing the performance of PhC cavities (particularly with respect to their radiative losses) is surely represented by the current lack of simple analytical (or even semianalytical) models linking the geometry of a cavity to the properties of its optical modes.

In the present paper, we show that such a model can be defined for L_N (and L_N-like) cavities as soon as $N>3$, i.e., as soon as their confined optical modes can be expanded in terms of the one-dimensional (1D) Bloch eigenstates of a PhC W1 waveguide [see Fig. 1(b)]. Coupled to their somewhat "softer" confinement along the main cavity axis, the possibility to write the localized (0D) modes of relatively long ($N>3$) L_N cavities in terms of a small number of extended (1D) W1-waveguide states suggests a parallel between these PhC defects and *shallow* impurities in semiconductors. Similarly to the case of shallow impurities, indeed, the expansion in waveguide eigenmodes can be used to extract important information on the fundamental properties of L_N cavity modes. More importantly, however, such an expansion can be used to find a direct relationship between the dielectric constant of a cavity and the spatial distribution of its modes, which can in turn be applied to the design of cavities supporting modes with *arbitrarily shaped field distributions*. The potentially high impact of this method on the field of PhC-cavity engineering is demonstrated in the final part of this work, where we describe the steps necessary to generate a cavity whose fundamental mode is characterized by a *Gaussian* envelope function[23] and by ultralow radiative losses (as attested to by a Q factor of 17.5×10^6).

II. EXPANSION OF PhC CAVITY MODES IN WAVEGUIDE EIGENSTATES

The first step toward the formulation of a method to design PhC cavities having the desired mode distribution is to find the correct way to expand the mth mode of a generic L_N cavity, $\vec{E}_N^m(x,y)$, in terms of the 1D Bloch eigenmodes of a PhC W1 structure with the same r/a and membrane thickness. In general terms, such an expansion should take the form

$$\vec{E}_N^m(x,y)=\frac{1}{\sqrt{V}}\sum_n\sum_{k_x}^{0,2\pi/a} c_{nk_x}^{m,N}\vec{E}^{nk_x}(x,y)e^{ik_xx}. \quad (1)$$

Here, V is the domain volume, the waveguides modes are written as $\vec{E}^{nk_x}(x,y)e^{ik_xx}$ [see Fig. 1(d) for some examples], and the sum in k_x is centered on the minimum of the W1 band of interest ($k_x=\pi/a$). The modes of the PhC waveguide, as well as those of the L_N cavities, are obtained here from 2D finite-difference (2DFD) computations,[24] in the effective-index approximation[25] and with periodic boundary conditions (in the case of the waveguide). The effective index used in the computations ($n_{\text{eff}}=3.223$) is determined by matching the frequency of the fundamental mode of a GaAs-based L_3 test cavity computed in 2D to the result of a full three-dimensional (3D) finite-difference time-domain (FDTD) computation,[26] performed on the same cavity embedded in a GaAs slab with thickness $t=265$ nm (compatible with the integration of site-controlled pyramidal QDs (Refs. 20 and 27) and V-groove quantum wires[28]). The GaAs refractive index at $T=10$ K and $\lambda_0\approx870$ nm ($n_{\text{GaAs}}\approx3.518$) (Ref. 29) is used in the 3D FDTD calculations. By using n_{eff} in the 2D model, it is possible to account for the finite extension of the real (i.e., inherently 3D) cavity modes in the out-of-plane (z) direction. In the limited range of frequencies considered here ($\sim0.22c/a-0.27c/a$, roughly corresponding to the extension of the guided PhC W1 bands) n_{eff} is found to be nearly constant, and independent of the specific PhC cavity geometry; as a consequence, the same index value can be used throughout the calculations for both the W1 waveguide and the L_N cavities.[25] The near-infrared dispersion of n_{GaAs} is taken into account *a posteriori*, by properly correcting the eigenfrequencies obtained from the 2D model.

It should be noted that the first sum in Eq. (1) extends over all the $n(\rightarrow\infty)$ bands of the PhC dispersion [see Fig. 1(c)]. For specific modes of the cavity, however, the number of bands over which the sum is performed can be drastically reduced, by taking into account the symmetry, the spatial localization and the energy position of the mode with respect to the band diagram of the waveguide [displayed in Fig. 1(c)]. For calculating the L_N-cavity modes, in particular, the sum in Eq. (1) can be limited to the bands that are actually confined in the W1 waveguide, with the additional constraint that the spatial symmetry of the band states must match that of the cavity mode under scrutiny. This means that if we focus our attention on the cavity modes that are *odd* with respect to reflection about the x-z plane (for L_N cavities the fundamental mode belongs to this particular class), we only

have to take into account the lowest guided band [see Fig. 1(c)]. Hence, Eq. (1) reduces to

$$\vec{E}_N^m(x,y) = \frac{1}{\sqrt{V}} \sum_{k_x}^{0,2\pi/a} c_{\mathrm{w}k_x}^{m,N} \vec{E}^{\mathrm{w}k_x}(x,y) e^{ik_x x}, \tag{2}$$

where the band index n was dropped in favor of the constant label w.

In order to be able to use Eq. (2) to actually reconstruct the L_N-cavity modes, an explicit expression for the $c_{\mathrm{w}k_x}^{m,N}$ coefficients must be found. To this end, we rewrite Eq. (2) in the limit $V \to \infty$,

$$\vec{E}_N^m(x,y) \overset{V\to\infty}{\to} \frac{1}{\sqrt{2\pi}} \int_0^{2\pi/a} c_{\mathrm{w}k_x}^{m,N} \vec{E}^{\mathrm{w}k_x}(x,y) e^{ik_x x} dk_x. \tag{3}$$

Equation (3) is a vectorial expression, valid for any component of the electric field; for $E_y^{m,N}(x,y)$, we have

$$E_y^{m,N}(x,y) = \frac{1}{\sqrt{2\pi}} \int_0^{2\pi/a} c_{\mathrm{w}k_x}^{m,N} E_y^{\mathrm{w}k_x}(x,y) e^{ik_x x} dk_x. \tag{4}$$

If both sides of Eq. (4) are integrated over y, we obtain

$$\mathcal{E}_y^{m,N}(x) = \frac{1}{\sqrt{2\pi}} \int_0^{2\pi/a} c_{\mathrm{w}k_x}^{m,N} \mathcal{E}_y^{\mathrm{w}k_x}(x) e^{ik_x x} dk_x \tag{5}$$

with

$$\mathcal{E}_y^{m,N}(x) = \int_{-\infty}^{\infty} E_y^{m,N}(x,y) dy \tag{6}$$

and

$$\mathcal{E}_y^{\mathrm{w}k_x}(x) = \int_{-\infty}^{\infty} E_y^{\mathrm{w}k_x}(x,y) dy. \tag{7}$$

The following step is to express $\mathcal{E}_y^{m,N}(x)$ in terms of its Fourier transform (FT) so that Eq. (5) becomes

$$\frac{1}{\sqrt{2\pi}} \int_{-\infty}^{\infty} \mathrm{FT}\{\mathcal{E}_y^{m,N}(x)\}|_{k_x} e^{ik_x x} dk_x = \frac{1}{\sqrt{2\pi}} \int_0^{2\pi/a} c_{\mathrm{w}k_x}^{m,N} \mathcal{E}_y^{\mathrm{w}k_x}(x) e^{ik_x x} dk_x. \tag{8}$$

Before proceeding further, we must note that the functions $\mathcal{E}_y^{\mathrm{w}k_x}(x)e^{ik_x x}$ are solutions to the following *one-dimensional* wave equation:

$$-\frac{\partial^2[\mathcal{E}_y^{\mathrm{w}k_x}(x)e^{ik_x x}]}{\partial x^2} = \left(\frac{\omega_{\mathrm{w}k_x}}{c}\right)^2 \varepsilon_{\mathrm{w}}^{1\mathrm{D}}(x) \mathcal{E}_y^{\mathrm{w}k_x}(x) e^{ik_x x}, \tag{9}$$

where $\omega_{\mathrm{w}k_x}$ is the frequency of the odd W1 band in k_x [see Fig. 1(c)], and $\varepsilon_{\mathrm{w}}^{1\mathrm{D}}(x)$ is an effective 1D dielectric constant for the waveguide. $\varepsilon_{\mathrm{w}}^{1\mathrm{D}}(x)$ can be evaluated from the two-dimensional dielectric constant, $\varepsilon_{\mathrm{w}}(x,y)$, by properly manipulating the explicit expression of the 2D wave equation,

$$\begin{cases} \dfrac{\partial^2(E_y^{\mathrm{w}k_x}e^{ik_x x})}{\partial y\,\partial x} - \dfrac{\partial^2(E_x^{\mathrm{w}k_x}e^{ik_x x})}{\partial y^2} = \left(\dfrac{\omega_{\mathrm{w}k_x}}{c}\right)^2 \varepsilon_{\mathrm{w}} \cdot E_x^{\mathrm{w}k_x} e^{ik_x x} \\ \dfrac{\partial^2(E_x^{\mathrm{w}k_x}e^{ik_x x})}{\partial x\,\partial y} - \dfrac{\partial^2(E_y^{\mathrm{w}k_x}e^{ik_x x})}{\partial x^2} = \left(\dfrac{\omega_{\mathrm{w}k_x}}{c}\right)^2 \varepsilon_{\mathrm{w}} \cdot E_y^{\mathrm{w}k_x} e^{ik_x x} \end{cases}. \tag{10}$$

[Here, we temporarily dropped the (x,y) dependence for $E_i^{\mathrm{w}k_x}(x,y)$ and for $\varepsilon_{\mathrm{w}}(x,y)$.]

If both sides of the bottommost equation contained in Eq. (10) are integrated over y, we get

$$-\frac{\partial^2[\mathcal{E}_y^{\mathrm{w}k_x}(x)e^{ik_x x}]}{\partial x^2} = \left(\frac{\omega_{\mathrm{w}k_x}}{c}\right)^2 \left[\int_{-\infty}^{\infty} \varepsilon_{\mathrm{w}}(x,y) \cdot E_y^{\mathrm{w}k_x}(x,y) dy\right] e^{ik_x x}. \tag{11}$$

By comparing Eqs. (9) and (11), we easily obtain

$$\varepsilon_{\mathrm{w}}^{1\mathrm{D}}(x) = \frac{\int_{-\infty}^{\infty} \varepsilon_{\mathrm{w}}(x,y) \cdot E_y^{\mathrm{w}k_x}(x,y) dy}{\int_{-\infty}^{\infty} E_y^{\mathrm{w}k_x}(x,y) dy [= \mathcal{E}_y^{\mathrm{w}k_x}(x)]}. \tag{12}$$

Such an expression for $\varepsilon_{\mathrm{w}}^{1\mathrm{D}}(x)$ is actually quite reasonable, since it means that the effective 1D dielectric constant we were looking for is given by the integral over y of the two-dimensional $\varepsilon_{\mathrm{w}}(x,y)$, weighted by its overlap with the periodic part of the waveguide modes. Now that we have $\varepsilon_{\mathrm{w}}^{1\mathrm{D}}(x)$, we can use the orthonormality condition for solutions of Eq. (9),[30]

$$\int_{-\infty}^{\infty} [\varepsilon_{\mathrm{w}}^{1\mathrm{D}}(x)]^{1/2} \mathcal{E}_y^{\mathrm{w}k_x}(x) \cdot \{[\varepsilon_{\mathrm{w}}^{1\mathrm{D}}(x)]^{1/2} \mathcal{E}_y^{\mathrm{w}k_x'}(x)\}^* e^{i(k_x - k_x')x} dx = 2\pi\delta(k_x - k_x'), \tag{13}$$

to obtain the $c_{\mathrm{w}k_x}^{m,N}$ coefficients. To this end, we multiply both sides of Eq. (8) by $\frac{1}{\sqrt{2\pi}}[\varepsilon_{\mathrm{w}}^{1\mathrm{D}}(x)]^{1/2} \cdot \{[\varepsilon_{\mathrm{w}}^{1\mathrm{D}}(x)]^{1/2} \cdot [\mathcal{E}_y^{\mathrm{w}k_x'}(x)e^{ik_x' x}]\}^*$ and we integrate over x, getting

$$\frac{1}{2\pi} \int_{-\infty}^{\infty} \int_{-\infty}^{\infty} \mathrm{FT}[\mathcal{E}_y^{m,N}(x)]|_{k_x} \cdot [\varepsilon_{\mathrm{w}}^{1\mathrm{D}}(x)]^{1/2} \cdot \{[\varepsilon_{\mathrm{w}}^{1\mathrm{D}}(x)]^{1/2} \cdot [\mathcal{E}_y^{\mathrm{w}k_x'}(x)]\}^* e^{i(k_x - k_x')x} dk_x dx = c_{\mathrm{w}k_x'}^{m,N}. \tag{14}$$

Now, since $[\mathcal{W}_y^{\mathrm{w}k_x'}(x)]^* = [\varepsilon_{\mathrm{w}}^{1\mathrm{D}}(x)]^{1/2} \cdot \{[\varepsilon_{\mathrm{w}}^{1\mathrm{D}}(x)]^{1/2} \cdot [\mathcal{E}_y^{\mathrm{w}k_x'}(x)]\}^*$ is a periodic function in a, we can write

$$[\mathcal{W}_y^{\mathrm{w}k_x'}(x)]^* = \sum_G (\mathcal{W}_G^{\mathrm{w}k_x'})^* \cdot e^{-iG\cdot x}. \tag{15}$$

G $[= \pm(2\pi/a)m$, with $m = 0,1,\ldots,\infty]$ is the 1D reciprocal lattice vector, and for $\mathcal{W}_G^{\mathrm{w}k_x'}$ the following relationship holds true:

$$(\mathcal{W}_G^{\mathrm{wk}_x'})^* = \frac{1}{a}\int_{-a/2}^{a/2} [\mathcal{W}_y^{\mathrm{wk}_x'}(x)]^* e^{iG\cdot x} dx. \tag{16}$$

Substituting Eq. (15) in Eq. (14), we have

$$\frac{1}{2\pi}\sum_G \int_{-\infty}^{\infty}\int_{-\infty}^{\infty} \mathrm{FT}\{\mathcal{E}_y^{m,N}(x)\}|_{k_x} \cdot (\mathcal{W}_G^{\mathrm{wk}_x'})^* e^{i[k_x-(k_x'+G)]x} dk_x dx = c_{\mathrm{wk}_x'}^{m,N}, \tag{17}$$

that is,

$$\sum_G \int_{-\infty}^{\infty} \mathrm{FT}[\mathcal{E}_y^{m,N}(x)]|_{k_x} \cdot (\mathcal{W}_G^{\mathrm{wk}_x'})^* \delta[k_x - (k_x' + G)] dk_x = c_{\mathrm{wk}_x'}^{m,N}. \tag{18}$$

Finally, we obtain

$$c_{\mathrm{wk}_x}^{m,N} = \sum_G \mathrm{FT}\{\mathcal{E}_y^{m,N}(x)\}|_{(k_x+G)} \cdot (\mathcal{W}_G^{\mathrm{wk}_x})^* \tag{19}$$

(where we have replaced the index k_x' with k_x).

The expression of the $c_{\mathrm{wk}_x}^{m,N}$ coefficients provided in Eq. (19) is composed of two terms, which must be evaluated separately. Namely, these two terms are (i) the 1D Fourier transform of the L_N cavity mode, $\mathrm{FT}\{\mathcal{E}_y^{m,N}(x)\}|_{k_x+G}$, and (ii) the $\mathcal{W}_G^{\mathrm{wk}_x}$ term, which depends solely on the dielectric constant and eigenmodes of the waveguide. The absolute value of the 1D FT of the fundamental mode (M_0) of the L_5 cavity, $\mathrm{FT}\{\mathcal{E}_y^{0,5}(x)\}|_{k_x+G}$, is shown in Fig. 2(a) as an example of (i). It is interesting to note that more than 98% of the 1D FT of this mode is comprised within the interval $k_x \in [-\frac{4\pi}{a}, \frac{4\pi}{a}]$, and that similar percentages characterize all the modes studied in the present work. This observation, coupled to the fact that the values assumed by $\mathcal{W}_G^{\mathrm{wk}_x}$ become negligible for $|G| > \frac{8\pi}{a}$ [see Fig. 2(b)], allows us to safely truncate the sum in Eq. (19) at $G = \pm\frac{8\pi}{a}$ when trying to evaluate the $c_{\mathrm{wk}_x}^{m,N}$ coefficients. Since these coefficients provide the distribution of $\vec{E}_N^m(x,y)$ in the space of 1D Bloch modes of the PhC waveguide, following their evolution with increasing N can help our understanding of the nature of light confinement in L_N cavities. As shown in Fig. 2(c), indeed, the $c_{\mathrm{wk}_x}^{m,N}$ coefficients progressively localize around specific points of k_x space as the length of the cavity is increased, finally reconstructing the waveguide dispersion for $N \to \infty$. The frequency of the fundamental cavity mode, in particular, quickly approaches that of the minimum of the waveguide dispersion with increasing N, as a consequence of the reduced mode localization along the x axis (that is, the main axis of the cavity). The effects of this 0D→1D transition, which was studied both theoretically and experimentally in Ref. 31, are already apparent for relatively small values of N [e.g., $N=9-15$ in Fig. 2(c)]. The fact that even PhC cavities formed by 10–20 missing holes possess a well-defined "waveguidelike" character is at the origin of a recent proposal to use these cavities—coupled to single site-controlled QDs (Refs. 20 and 27)–as efficient "on chip" single photon guns.[32] The early onset of delocalization along the x axis for the optical modes of the L_N cavities is also confirmed by the excellent quality of the mode reconstruction obtained using Eqs. (2) and (19). In the following section, we will indeed show that such reconstruction becomes extremely accurate as soon as $N > 3$. As, for example, in the case of donors in semiconductors, the possibility to reconstruct a localized state (the cavity mode) as a linear combination of a reasonably small number of delocalized functions (the "odd" W1 Bloch eigenfunctions) can be interpreted as evidence of the *shallow* character of the PhC defects under consideration. The capability of writing a semianalytical expression for the k_x-space distribution of the modes associated with such "shallow cavities" opens the

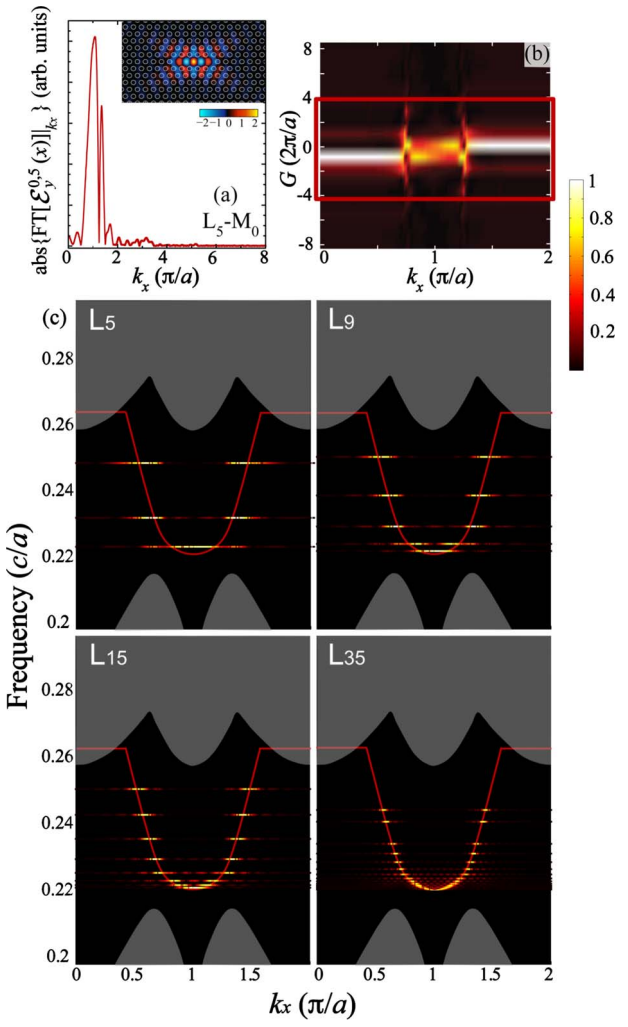

FIG. 2. (Color online) (a) Absolute value of $\mathrm{FT}\{\mathcal{E}_y^{m,N}(x)\}|_{k_x}$ for the fundamental mode (M_0) of the L_5 cavity (the function is symmetric with respect to $k_x=0$). The spatial distribution of the E_y component of this mode (computed by 2DFD) is shown in the inset. (b) Absolute value of $\mathcal{W}_G^{\mathrm{wk}_x}$ (see definition in the text). The box delimits the range of values of $\mathcal{W}_G^{\mathrm{wk}_x}$ ($G \in [-4\cdot\frac{2\pi}{a}, 4\cdot\frac{2\pi}{a}]$) that were included in the sum in Eq. (19). (c) Absolute value of the $c_{\mathrm{wk}_x}^{m,N}$ coefficients for the modes of four L_N cavities ($N=5,9,15,35$), superimposed to the odd waveguide band (displayed as a continuous line). The continuum bands of the PhC are shaded in gray. The color map on the right side of the figure is used in both panels (b) and (c). For each value of m and N, the positioning of the $c_{\mathrm{wk}_x}^{m,N}$ coefficients along the frequency axis was determined by the corresponding mode frequency.

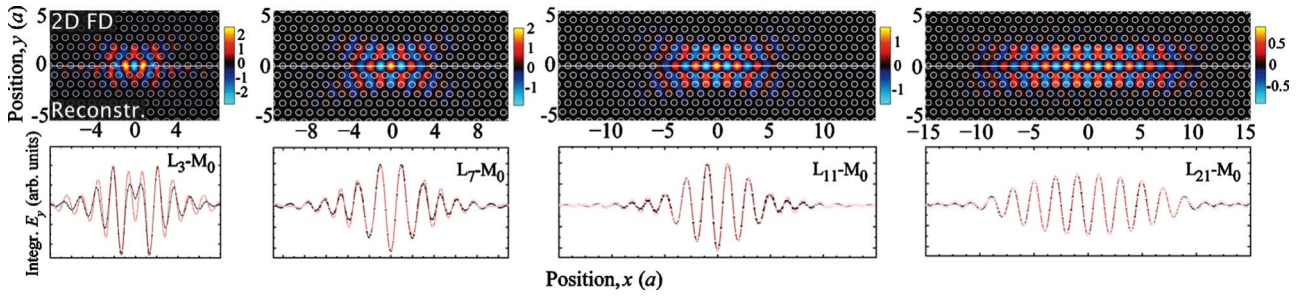

FIG. 3. (Color online) (Top) Spatial distribution of the E_y component of the fundamental mode (M_0) of four L_N cavities ($N=3,7,11,21$). The upper half shows the modes as obtained from 2D FD computations; in the lower half, the modes reconstructed using Eqs. (2) and (19) are displayed. (Bottom) Integral along y of the E_y component of the same modes shown in the top panel. The black dots connected by a black curve refer to the modes obtained from 2DFD computations; the white squares connected by a gray (red) curve to the modes obtained using Eqs. (2) and (19).

way to the direct engineering of the cavity properties. This intriguing possibility will be discussed in detail in the final section of the present work.

III. RECONSTRUCTION OF CAVITY MODES

In principle, the inclusion in Eq. (2) of the $c_{wk_x}^{m,N}$ coefficients given in Eq. (19) [and displayed in Fig. 2(c)] provides us with the means to reconstruct any mode of an arbitrary L_N cavity, as long as the mode is of the right parity (i.e., it is odd with respect to reflection about the x-z plane). In an attempt to test the limits to the validity of this approach, we applied Eqs. (2) and (19) to the fundamental mode (M_0) of a series of L_N cavities (a selection of the results obtained for $N=3,7,11,21,35$ is shown in the following), and compared the results of the reconstruction with the mode patterns computed by 2DFD. From the data summarized in Fig. 3, it is apparent that the match between the computed cavity modes and those obtained using Eqs. (2) and (19) is, in general, extremely good. Only for the L_3 cavity—the smallest structure studied here—one starts to notice sizeable differences between the reconstructed mode pattern and the computed one. Even though a good qualitative agreement is present even in this case, the reconstructed mode seems to be more extended than the computed one, suggesting an inherent difficulty of treating highly localized modes within our formalism. Continuing the parallel between L_N cavities and defects in semiconductors, this observation can be interpreted as evidence of an ongoing "shallow-to-deep defect" transition in L_N cavities with decreasing N. As we will see in the following, this transition is strictly connected to the broadening of the k_x-space distribution of the cavity modes taking place for $N \to 0$.

A first, potential hindrance to the reconstruction of highly localized cavity modes via Eq. (2) is indeed represented by the fact that the identification of the 1D Bloch modes belonging to the odd waveguide band becomes difficult as soon as these modes enter into resonance with the upper bands of the bulk photonic crystal (in gray in Figs. 1 and 2). For this reason, in the present work (i.e., for an r/a of 0.26, see Fig. 1) the W1 eigenstates corresponding to $k_x < k_0 (=0.4\frac{\pi}{a})$ and to $k_x > \frac{2\pi}{a} - k_0$ had to be approximated with $\vec{E}^{wk_0}(x,y)e^{ik_x x}$ and $\vec{E}^{w(-k_0)}(x,y)e^{-ik_x x}$, respectively. As long as N is sufficiently large, however, the $c_{wk_x}^{m,N}$ coefficients associated with these waveguide modes are very small [see Fig. 2(c)], and this approximation does not have any sizeable effects on the reconstruction of the cavity modes. When the cavity length is decreased, on the other hand, the modes become more and more confined along x, and the $c_{wk_x}^{m,N}$ coefficients progressively "spread out" in k_x space. Eventually, the weight of the approximated waveguide eigenstates becomes no longer negligible, leading to errors in the mode reconstruction. In addition, for very short cavities the basic hypothesis that allowed us to formulate the approach summarized by Eqs. (2) and (19)—i.e., that the eigenmodes of a PhC waveguide represent a *complete basis* for PhC-cavity modes—is no longer valid. In order to properly reconstruct the modes of such short cavities—which in many respects can indeed be likened to *deep defects* in semiconductors—we should in principle go all the way back to Eq. (1), to include all the PhC bands in the expansion of the cavity mode. Among other things, this would require the evaluation and the identification of the totality of the PhC states, rendering the reconstruction procedure extremely cumbersome and, ultimately, impractical.

As evidenced by the data reported in Fig. 3, however, for the L_N cavities such a shallow-to-deep defect transition does not occur until $N \leq 3$. Apart from confirming that a certain waveguidelike character is acquired by L_N cavities as soon as the cavity length exceeds a few unit cells, these results attest to the general validity of our approach. In Fig. 4, we display the results obtained by applying Eqs. (2) and (19) to a selection of the modes confined in an L_{35} cavity. As the data reported in the figure clearly demonstrate, our capability to correctly reconstruct L_N-cavity modes is not limited to the M_0 [Figs. 4(a) and 4(b)] but it also extends to the confined modes of higher frequency [Figs. 4(c)–4(h)].

IV. CAVITY DESIGN

As we saw in the previous Sections (as well as in Ref. 31), the capability to expand the modes of an L_N cavity in terms of the Bloch eigenstates of a W1 waveguide can provide interesting insight into the nature of light confinement in

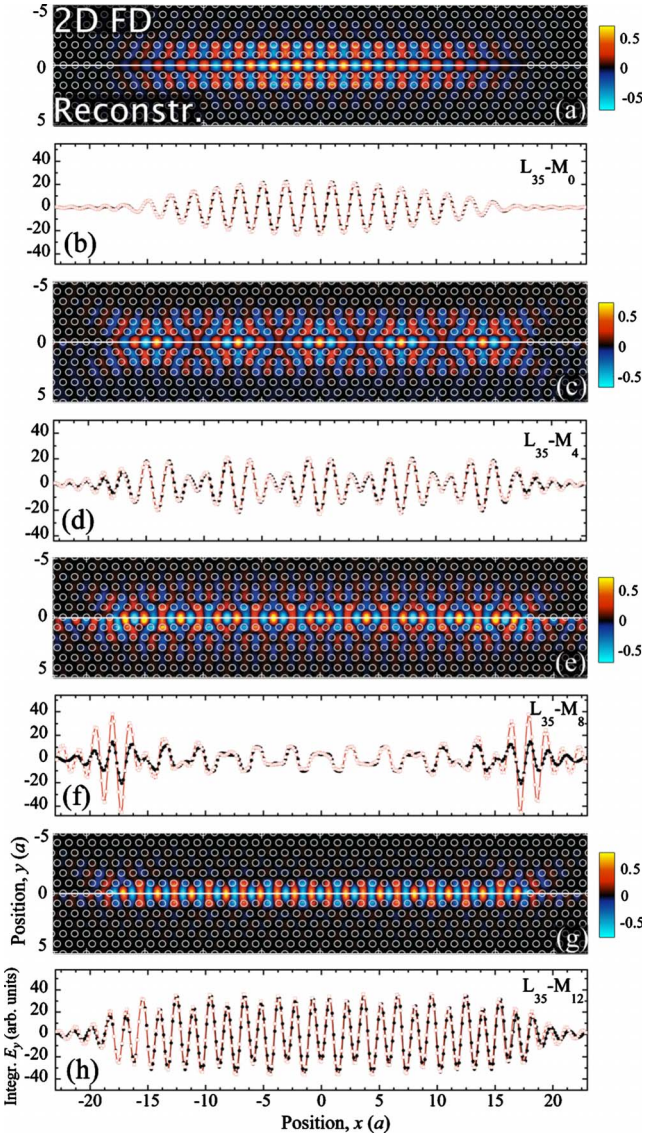

FIG. 4. (Color online) (a), (c), (e), and (g) Spatial distribution of the E_y component of four modes [(a)-M_0, (c)-M_4, (e)-M_8, (g)-M_{12}] of the L_{35} cavity. The upper half shows the modes as obtained from 2DFD computations; in the lower half, the modes reconstructed using Eqs. (2) and (19) are displayed. (b), (d), (f), and (h) Integral along y of the E_y component of the same modes shown in (a), (c), (e), and (g). The black dots connected by a black curve refer to the modes obtained from 2DFD computations; the white squares connected by a gray (red) curve to the modes obtained using Eqs. (2) and (19).

PhC defects, in particular with respect to the *dimensionality* (0D or 1D) of the photonic wave functions. In the following paragraphs, we will demonstrate that the formalism developed in Sec. II can have a second, much more practical, application: it can be used to design PhC cavities that support optical modes with *predefined properties* while also being compatible with state-of-the-art fabrication techniques. As a proof of principle for the feasibility of this approach, in the final part of this section we will discuss the properties of a PhC cavity engineered to support a mode with Gaussian envelope function and ultralow radiative losses. In order to get to this point, however, we have to find a way to express the dielectric constant of an arbitrary PhC cavity in terms of the spatial distribution of its fundamental confined mode. To this end, it is first of all necessary to rewrite Eq. (2) for such a generic, initially unknown PhC cavity, henceforth labeled as "X,"

$$\vec{E}^0_{\mathrm{X}}(x,y) = \frac{1}{\sqrt{V}} \sum_{k_x}^{0,2\pi/a} c^{0,\mathrm{X}}_{\mathrm{wk}_x} \vec{E}^{\mathrm{wk}_x}(x,y) e^{ik_x x}. \tag{20}$$

Of course, the conditions for the validity of Eq. (20) are identical to those holding for Eq. (2), that is, (i) the reconstructed mode must have the right parity and (ii) light confinement along x must be weaker than that typical of the modes of an L_3 cavity.

The electric field associated with the cavity mode, $\vec{E}^0_{\mathrm{X}}(x,y)$, is a solution of the following wave equation:

$$\vec{\nabla} \times [\vec{\nabla} \times \vec{E}^0_{\mathrm{X}}(x,y)] = \left(\frac{\omega^0_{\mathrm{X}}}{c}\right)^2 \varepsilon_{\mathrm{X}}(x,y) \vec{E}^0_{\mathrm{X}}(x,y), \tag{21}$$

where ω^0_{X} is the frequency of the mode. If we replace $\vec{E}^0_{\mathrm{X}}(x,y)$ with its expansion in waveguide modes [see Eq. (20)], we obtain

$$\sum_{k_x}^{0,2\pi/a} c^{0,\mathrm{X}}_{\mathrm{wk}_x} \{\vec{\nabla} \times [\vec{\nabla} \times \vec{E}^{\mathrm{wk}_x}(x,y) e^{ik_x x}]\} = \left(\frac{\omega^0_{\mathrm{X}}}{c}\right)^2 \varepsilon_{\mathrm{X}}(x,y) \sum_{k_x}^{0,2\pi/a} c^{0,\mathrm{X}}_{\mathrm{wk}_x} \vec{E}^{\mathrm{wk}_x}(x,y) e^{ik_x x}. \tag{22}$$

Since the waveguide eigenmodes, $\vec{E}^{\mathrm{wk}_x}(x,y)e^{ik_x x}$, are the solutions of the W1 wave equation,

$$\vec{\nabla} \times [\vec{\nabla} \times \vec{E}^{\mathrm{wk}_x}(x,y) e^{ik_x x}] = \left(\frac{\omega_{\mathrm{wk}_x}}{c}\right)^2 \varepsilon_{\mathrm{w}}(x,y) \vec{E}^{\mathrm{wk}_x}(x,y) e^{ik_x x}, \tag{23}$$

we can rewrite Eq. (22) as

$$\varepsilon_{\mathrm{w}}(x,y) \cdot \sum_{k_x}^{0,2\pi/a} c^{0,\mathrm{X}}_{\mathrm{wk}_x} \cdot (\omega_{\mathrm{wk}_x})^2 \cdot \vec{E}^{\mathrm{wk}_x}(x,y) e^{ik_x x} = (\omega^0_{\mathrm{X}})^2 \varepsilon_{\mathrm{X}}(x,y) \sum_{k_x}^{0,2\pi/a} c^{0,\mathrm{X}}_{\mathrm{wk}_x} \vec{E}^{\mathrm{wk}_x}(x,y) e^{ik_x x}. \tag{24}$$

By taking the absolute value of the y component of both sides of this vectorial equation, we get

$$\varepsilon_{\mathrm{w}}(x,y) \cdot \left| \sum_{k_x}^{0,2\pi/a} c^{0,\mathrm{X}}_{\mathrm{wk}_x} \cdot (\omega_{\mathrm{wk}_x})^2 \cdot E_y^{\mathrm{wk}_x}(x,y) e^{ik_x x} \right| = (\omega^0_{\mathrm{X}})^2 \varepsilon_{\mathrm{X}}(x,y) \left| \sum_{k_x}^{0,2\pi/a} c^{0,\mathrm{X}}_{\mathrm{wk}_x} E_y^{\mathrm{wk}_x}(x,y) e^{ik_x x} \right|, \tag{25}$$

provided that we want $\varepsilon_{\mathrm{X}}(x,y)$ to only take real, positive values. From Eq. (25), the following expression of $\varepsilon_{\mathrm{X}}(x,y)$ can be easily obtained:

$$\varepsilon_X(x,y) = \varepsilon_w(x,y) \cdot \frac{\left| \sum_{k_x}^{0,2\pi/a} c_{wk_x}^{0,X} \cdot (\omega_{wk_x})^2 \cdot E_y^{wk_x}(x,y) e^{ik_x x} \right|}{(\omega_X^0)^2 \cdot \left| \sum_{k_x}^{0,2\pi/a} c_{wk_x}^{0,X} E_y^{wk_x}(x,y) e^{ik_x x} \right|}. \quad (26)$$

In Eq. (26), the $c_{wk_x}^{0,X}$ coefficients are obtained via Eq. (19) while $\vec{E}^{wk_x}(x,y)e^{ik_x x}$ and ω_{wk_x} are evaluated by solving Eq. (23) with the 2DFD method. In the intervals $k_x < k_0$ ($=0.4\frac{\pi}{a}$ for an r/a of ~ 0.26) and $k_x > \frac{2\pi}{a} - k_0$, where the odd waveguide band is resonant with the upper PhC bands, the W1 eigenmodes are approximated as described in Sec. III while ω_{wk_x} is taken to be equal to ω_{wk_0} [see the band sketched as a continuous line in Fig. 2(c)]. The frequency of the X cavity mode, ω_X^0, is treated as a normalization constant, fixed by the condition $\varepsilon_X(0,0) = \varepsilon_{GaAs}$ (where ε_{GaAs} is the effective dielectric constant of the GaAs slab at the wavelength of the cavity mode).

Even though Eq. (26) provides the necessary link between $\varepsilon_X(x,y)$ and the field distribution of the cavity mode, it does not yet fulfill our goal of designing a realistic PhC cavity supporting $\vec{E}_X^0(x,y)$. This is due to the fact that the expression of $\varepsilon_X(x,y)$ given in Eq. (26) can take any positive value, whereas the most convenient way of fabricating a PhC cavity in a membrane configuration is by etching air holes in the GaAs slab. As a consequence, it is necessary to find a way to define an *effective* dielectric constant, retaining the properties of $\varepsilon_X(x,y)$ in spite of only taking two values: 1 (the dielectric constant of air) and ε_{GaAs}. A possible way to accomplish this goal involves the evaluation of the average of $\varepsilon_X(x,y)$ over each unit cell of the PhC,[33]

$$\langle \varepsilon_X \rangle (x_i, y_i) = \frac{1}{a^2} \int_{-a/2}^{a/2} \int_{-a/2}^{a/2} \varepsilon_X(x - x_i, y - y_i) dx dy, \quad (27)$$

where x_i and y_i are the coordinates of the center of each PhC hole in the original waveguide dielectric constant, $\varepsilon_w(x,y)$. In a PhC structure fabricated by drilling holes in GaAs, there exists a simple relationship between $\langle \varepsilon_X \rangle (x_i, y_i)$ and the r/a of the hole contained in each unit cell,

$$\langle \varepsilon_X \rangle (x_i, y_i) = \varepsilon_{GaAs} - \pi (r_i/a)^2 \cdot (\varepsilon_{GaAs} - 1). \quad (28)$$

For a generic $\varepsilon_X(x,y)$ obtained from Eq. (26), the relationship provided in Eq. (28) allows for defining an *equivalent* dielectric constant, whose average in each unit cell is set to the value of $\langle \varepsilon_X \rangle (x_i, y_i)$ by properly tuning the radius (r_i) of the corresponding hole. As we will see in the following, this is usually sufficient to reproduce the main properties of a cavity defined through Eq. (26). In particular, the fundamental mode supported by the cavity obtained from Eq. (28) is generally identical to $\vec{E}_X^0(x,y)$.

It is important to mention, however, that in some instances it is impossible to correctly reproduce $\langle \varepsilon_X \rangle (x_i, y_i)$ through simple adjustments of r_i. In these situations, additional approximations have to be performed. If, for example, $\langle \varepsilon_X \rangle (x_i, y_i)$ is larger than ε_{GaAs} (the maximum value that can be taken by the dielectric constant in a GaAs slab), no hole is placed in the unit cell; if, on the other hand, $\langle \varepsilon_X \rangle (x_i, y_i)$ is smaller than 1, the unit cell is filled with air. An additional situation in which no hole is inserted within a given unit cell occurs whenever the required hole radius is too small to be fabricated—i.e., when the value of $\langle \varepsilon_X \rangle (x_i, y_i)$ is too close to ε_{GaAs}. For the cavity discussed at the end of this section, the lower limit for r_i was set to 30 nm. Of course, any of these approximations introduces a local discrepancy between the average dielectric constant of our "realistic" cavity and the value of $\langle \varepsilon_X \rangle (x_i, y_i)$ estimated from Eq. (27). The effects of such a discrepancy on the properties of the modes supported by the cavity can be rather significant, if the unit cells subject to the approximation are characterized by a high intensity of the confined electromagnetic field. For this reason, whenever one of the three situations listed above is verified in any of the unit cells positioned along the main axis of the cavity (at $y=0$), the local deviation from $\langle \varepsilon_X \rangle (x_i, y_i)$ is corrected by properly adjusting the radius of the neighboring holes.

Now that we have outlined a method to "extract" the geometrical properties of a PhC cavity from the spatial distribution of its confined modes, we wish to test this approach through the design of a structure with potentially interesting properties. As mentioned in Sec. I, in recent years the problem of the minimization of radiative losses in PhC membrane cavities has been the object of extensive research.[21–23,33–37] When approaching this topic, it is first of all necessary to remember that PhC membranes exploit two fundamentally diverse mechanisms to confine photons along different spatial directions. While in the plane of the slab light confinement is indeed provided by the PhC lattice (and can thus be made arbitrarily strong by increasing the crystal size), in the vertical direction one has to completely rely on total internal reflection (TIR) at the slab-air interface. For this reason, the $\vec{k}$ components of the electromagnetic field that fall into the so-called *light cone*—i.e., that do not respect the TIR condition ($|\vec{k}| \geq \frac{2\pi}{\lambda_0}$, λ_0 being the photon wavelength in air)—are free to propagate outside the slab. Since this fact alone accounts for nearly all of the cavity losses, it is not surprising to discover that virtually every method proposed to achieve high-Q factors is based on the suppression of the *light-cone components* of the fundamental mode of the cavity of interest.[21–23,33–37] To this date, most of these methods have relied on rather lengthy parameter-space scans, performed by means of 3D FDTD simulations[21–23,34–36] or, in Ref. 37, by using a conjugate gradient search algorithm. Only in one case,[33] an attempt was made to explicitly derive a semianalytical relationship between the mode distribution and the dielectric constant of the cavity. However, this was achieved at the expense of a series of rather severe approximations, eventually resulting in a dielectric constant-cavity mode relationship that is only defined near $y=0$ (i.e., along the main cavity axis). This is radically different from what we can achieve with our method, which allows us to accurately map the dielectric constant of the cavity in the entire x-y plane, without resorting to any major approximations.

Following the proposal made by Akahane *et al.* in Ref. 21, we will now try to apply our method to the design of a PhC membrane cavity supporting a mode with *Gaussian* envelope function. The reasons for studying this particular cav-

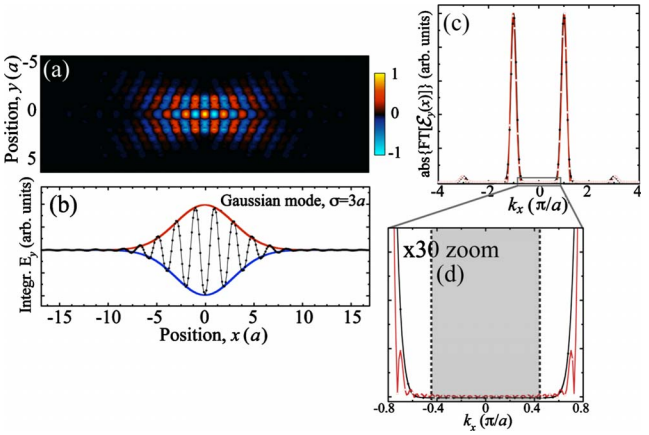

FIG. 5. (Color online) (a) Spatial distribution of the E_y component of a mode with Gaussian envelope function ($\sigma=3a$), reconstructed as described in the main text. (b) Integral along y of the E_y component shown in (a). Two Gaussian curves corresponding to $\sigma=3a$ are plotted for comparison as continuous (red and blue) lines. (c) Comparison between the absolute value of the 1D Fourier Transform $(\mathrm{FT}\{\mathcal{E}_y(x)\}|_{k_x})$ of the ideal Gaussian mode defined by Eq. (29) (black dots connected by a black curve) and of the reconstructed mode shown in (a) and (b) [white squares connected by a gray (red) curve.] (d) 30× zoom of (c) in the *light-cone* region (shaded in light gray in the figure).

ity mode reside in the peculiar properties of its $\vec{k}$-space distribution, which can be adjusted to achieve virtually zero light-cone components (and, thus, ultrahigh Q factors). Such a mode can be easily defined by multiplying the PhC W1 eigenmode in $k_x=\pi/a$—the minimum of the waveguide band—by a Gaussian function,

$$\vec{E}^0_{\mathrm{X}}(x,y)=\vec{E}^{\mathrm{w},\pi/a}(x,y)e^{i(\pi/a)x-x^2/2\sigma_x^2}, \tag{29}$$

where σ_x determines the spatial extent of the confined field. As displayed in Fig. 5(c), the 1D Fourier transform of $\vec{E}^0_{\mathrm{X}}(x,y)$ is composed of a series of Gaussian peaks, centered at $k_x=\pm\pi/a+G$ and with standard deviation $\sigma_{k_x}=\frac{1}{\pi\sigma_x}(\frac{\pi}{a})$. If the value of σ_x is set to $3a$—as was done in the present work—the light-cone components of the mode become indeed negligible [see Fig. 5(d)]. In addition, for this value of σ_x the reconstruction of $\vec{E}^0_{\mathrm{X}}(x,y)$ via Eq. (20) is extremely accurate, in both real and $\vec{k}$ space (see Fig. 5). As we will see in the following, such a high accuracy results in the possibility to correctly estimate—through the application of Eqs. (26) and (28)—the dielectric constant distribution of the X cavity supporting the Gaussian mode defined in Eq. (29). In Fig. 6(a), we present the X cavity obtained with our method, superimposed on a false-color mapping of the hole r/a. Even though it is perhaps difficult to appreciate the hole-to-hole variations with the naked eye, the hole size varies by more than 25% throughout the cavity. If rescaled to the value of a used in this work ($a=198$ nm), this variation corresponds to a spread of ~13 nm in the hole radius. This observation confirms the possibility to fabricate such a structure with remarkable precision, given that state-of-the-art e^--beam li-

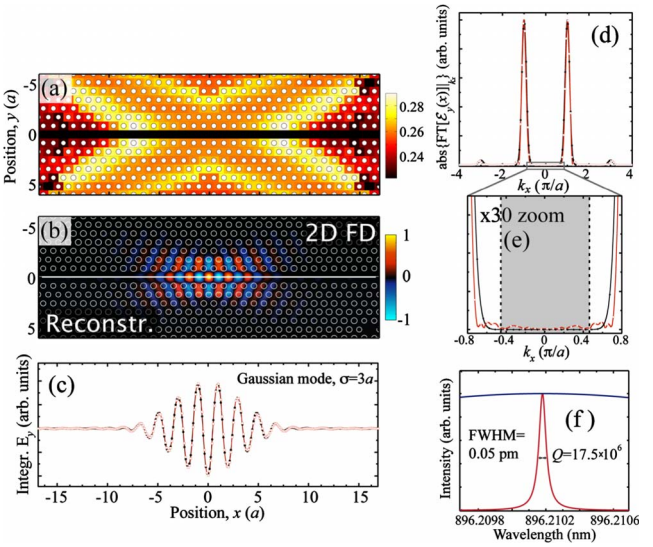

FIG. 6. (Color online) (a) False-color mapping of the radius r (in units of a, see color bar on the right) of the holes forming the X cavity defined in the main text. The holes are also shown, as circles of varying radius (proportional to the actual r). (b) Spatial distribution of the E_y component of the Gaussian mode supported by the X cavity presented in (a). The upper half shows the fundamental mode of the X cavity, as obtained from 2DFD computations. A mode with Gaussian envelope function ($\sigma=3a$)—reconstructed using the method described in the main text—is displayed in the lower half [same as in Fig. 5(a)]. (c) Integral along y of the E_y component of the same mode shown in (b). The black dots connected by a black curve refer to the mode obtained from 2DFD computations; the white squares connected by a gray (red) curve to the reconstructed mode with Gaussian envelope function [see main text and Fig. 5(b)]. (d) Comparison between the absolute value of the 1D Fourier Transform $(\mathrm{FT}\{\mathcal{E}_y(x)\}|_{k_x})$ of the ideal Gaussian mode defined by Eq. (29) (black dots connected by a black curve) and of the fundamental mode of the X cavity [white squares connected by a gray (red) curve]. (e) 30× zoom of (d) in the *light-cone* region (shaded in light gray in the figure). (f) Spectrum of the fundamental mode of the X cavity, obtained from 3D FDTD [gray (red) curve]. The Q factor of the mode (17.5×10^6) is indicated. The spectrum of the fundamental mode of an L_{11} cavity with nearly identical mode volume (see main text) is also shown for comparison [black (dark blue) curve, the mode wavelength was shifted to match that of the X-cavity mode; only a small portion of the mode peak fits in the displayed spectral range].

thography systems allow for defining the radius of a PhC hole with a ~1 nm resolution.[38,39]

By solving the wave equation given in Eq. (21) with the 2DFD method, it is possible to compute the fundamental mode of the X cavity displayed in Fig. 6(a), and to compare its properties to those of the target Gaussian mode. As the results summarized in Figs. 6(b)–6(e) clearly show, the computed $\vec{E}^0_{\mathrm{X}}(x,y)$ reproduces a Gaussian field distribution remarkably well. Even the computed mode frequency ($=0.2227c/a$) matches the value of ω^0_{X} ($=0.2212c/a$) obtained from the normalization of Eq. (26) within an error of less than 1%

However, the final test of the success of our attempt to recreate an X cavity supporting a mode with Gaussian enve-

lope function and low radiative losses is represented by the evaluation of the cavity *Q factor*. This is achieved by performing a 3D FDTD simulation[26,40–42] on a membrane with $t=265$ nm, embedding the PhC structure shown in Fig. 6(a). For the fundamental cavity mode, such a simulation yields a Q factor of 17.5×10^6, with a frequency of $0.2209c/a$ and a mode volume of 2.3 $(\lambda_0/n_{\mathrm{GaAs}})^3$. The latter value is slightly smaller than the effective volume of the fundamental mode of an L_{11} cavity with similar r/a [=2.35 $(\lambda_0/n_{\mathrm{GaAs}})^3$], which by contrast has a Q factor of 1.7×10^5 (more than 100 times lower than the one estimated for the X-cavity mode). We would like to stress that the ultrahigh Q value obtained for our X cavity was achieved without resorting to any time-consuming explorations of the parameter space, nor to other trial-and-error procedures. Furthermore, our method is not limited to the design of a specific type of cavity; on the contrary, it allows for obtaining PhC structures supporting truly arbitrary field distributions. The only limitation in this sense is represented by the condition that the target cavity mode must be sufficiently "shallow" (i.e., delocalized along x) to be correctly reconstructed with the approach described in Sec. II. However, this condition hardly affects the generality of the proposed method, given that the "shallow-to-deep" defect transition discussed in Sec. III only occurs for cavities whose effective length is on the order of that of an L_3.

V. CONCLUSIONS

To conclude, we would like to stress that the results presented in this work have the potential to revert the current paradigm in the field of PhC cavity engineering, leading to a shift from a trial-and-error approach to the direct design of PhC structures supporting arbitrary mode distributions. As discussed in Sec. IV, this is accomplished through the definition of a *semianalytic relationship* between the desired field distribution and the dielectric constant of the corresponding PhC cavity. In turn, such a relationship can be established thanks to the development of a formalism allowing us to write the optical modes of L_N (and L_N-like) PhC cavities as a linear combination of the 1D Bloch eigenstates of their corresponding (same r/a and membrane thickness) W1 PhC waveguide (see Secs. II and III). Here, this method is applied to the design of a PhC cavity whose fundamental mode presents a Gaussian envelope function and ultralow cavity losses, as attested by the Q factor of 17.5×10^6 estimated by 3D FDTD. However, in the immediate future we plan to extend this approach to the engineering of PhC structures with more complex mode distributions, including cavities supporting modes with *sinc*[33] or *heaviside*[43] envelope functions, systems of coupled cavities,[44,45] and coupled waveguide-cavity systems for *on-chip* photon generation and transfer.[46] Within this framework, a particularly important challenge is represented by the design of PhC cavities with polarization-degenerate modes, which could be employed to increase the collection efficiency of the entangled-photon pairs emitted, e.g., by site-controlled, high-symmetry pyramidal QDs.[47]

ACKNOWLEDGMENTS

This work was supported by the Swiss National Science Foundation (SNSF). The authors would like to thank K. F. Karlsson for providing the code for 2D FD computations and for helpful discussions. Fruitful discussions with V. Savona are also gratefully acknowledged.

APPENDIX: RECONSTRUCTION OF EVEN CAVITY MODES

When developing our formalism for the reconstruction of the modes of an L_N-like cavity in terms of the Bloch eigenmodes of its corresponding PhC W1 waveguide, we restricted ourselves to the cavity modes that are odd with respect to reflection about the x-z plane. Given the odd character of the fundamental mode of line-defect cavities, this restriction does not have a discernible impact on the general validity of the method of cavity design introduced in Sec. IV. However, it is probably interesting to verify the applicability of our approach to the reconstruction of the cavity modes stemming from the "even" W1 waveguide band [see Fig. 1(c)]. In the following, we will indeed dem-

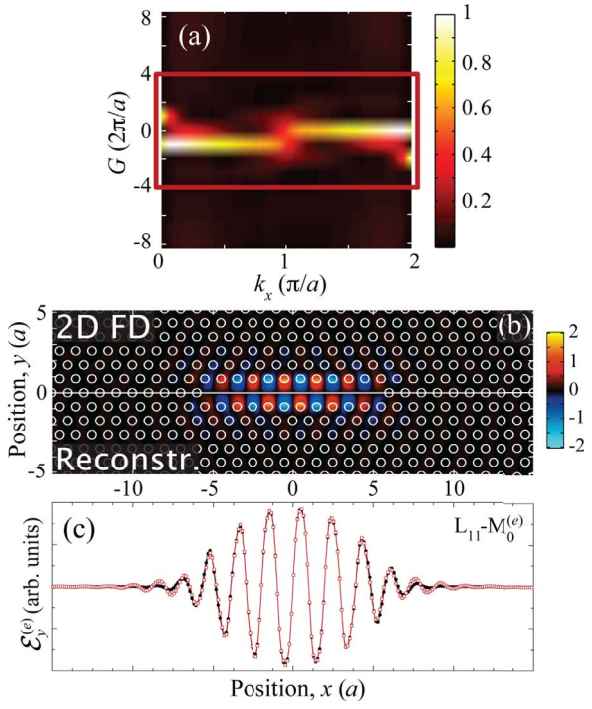

FIG. 7. (Color online) (a) Absolute value of $\mathcal{W}_G^{(e)\mathrm{w}k_x}$ (see definition in the text). The box delimits the range of values of $\mathcal{W}_G^{(e)\mathrm{w}k_x}$ ($G\in[-4\cdot\frac{2\pi}{a},4\cdot\frac{2\pi}{a}]$) that were included in the sum in Eq. (A4). (b) Spatial distribution of the E_y component of the lowest-frequency even mode ($\mathrm{M}_0^{(e)}$) supported by the L_{11} cavity. The upper half shows the mode as obtained from 2DFD computations; in the lower half, the mode reconstructed using Eqs. (2) and (A4) is displayed. (c) $\mathcal{E}_y^{(e)m,N}(x)$ (see definition in the text), calculated for the same mode shown in panel (b). The black dots connected by a black curve refers to the mode obtained from 2DFD computations; the white squares connected by a gray (red) curve to the mode obtained using Eqs. (2) and (A4).

onstrate that the evaluation of the $c_{\mathrm{wk}_x}^{m,N}$ coefficients for even cavity modes can proceed along the same lines discussed in Sec. II, provided that the obvious differences between cavity modes of opposite parity are properly taken into account. As a first step in this direction, it may be useful to rewrite Eq. (4),

$$E_y^{m,N}(x,y) = \frac{1}{\sqrt{2\pi}} \int_0^{2\pi/a} c_{\mathrm{wk}_x}^{m,N} E_y^{\mathrm{wk}_x}(x,y) e^{ik_x x} dk_x. \quad \text{(A1)}$$

For odd cavity modes (see Sec. II), it was possible to proceed further by integrating both sides of this equation along y [see Eqs. (5)–(7)]. For the y component of the electric field of an even PhC mode, however, the result of such an integral is equal to zero. In order to overcome this difficulty, a possibility is to define the following functions:

$$\mathcal{E}_y^{(e)m,N}(x) = \int_{-\infty}^{\infty} E_y^{m,N}(x,y)\mathrm{sgn}(y)dy \quad \text{(A2)}$$

and

$$\mathcal{E}_y^{(e)\mathrm{wk}_x}(x) = \int_{-\infty}^{\infty} E_y^{\mathrm{wk}_x}(x,y)\mathrm{sgn}(y)dy. \quad \text{(A3)}$$

If $\mathcal{E}_y^{m,N}(x)$ and $\mathcal{E}_y^{\mathrm{wk}_x}(x)$ are replaced with the above given expressions in the derivation laid out in Sec. II, it is relatively straightforward to demonstrate that for even cavity modes the $c_{\mathrm{wk}_x}^{m,N}$ coefficients take the form

$$c_{\mathrm{wk}_x}^{m,N} = \sum_G \mathrm{FT}\{\mathcal{E}_y^{(e)m,N}(x)\}|_{(k_x+G)} \cdot (\mathcal{W}_G^{(e)\mathrm{wk}_x})^* \quad \text{(A4)}$$

with

$$\mathcal{W}_G^{(e)\mathrm{wk}_x} = \frac{1}{a}\int_{-a/2}^{a/2} \{[\varepsilon_{\mathrm{w}}^{(e)1\mathrm{D}}(x)]^{1/2}\}^* \cdot [\varepsilon_{\mathrm{w}}^{(e)1\mathrm{D}}(x)]^{1/2} \cdot [\mathcal{E}_y^{(e)\mathrm{wk}_x}(x)] \cdot e^{-iG\cdot x} dx. \quad \text{(A5)}$$

Analogously to the case of odd cavity modes, the effective 1D dielectric constant, $\varepsilon_{\mathrm{w}}^{(e)1\mathrm{D}}(x)$, can be obtained by properly manipulating the 2D wave equations given in Eq. (10). For the even modes, we get

$$\varepsilon_{\mathrm{w}}^{(e)1\mathrm{D}}(x) = \frac{\int_{-\infty}^{\infty} \varepsilon_{\mathrm{w}}(x,y) \cdot E_y^{\mathrm{wk}_x}(x,y)\mathrm{sgn}(y)dy}{\mathcal{E}_y^{(e)\mathrm{wk}_x}(x)} + \frac{2\frac{\partial}{\partial x}[E_x^{\mathrm{wk}_x}(x,0)e^{ik_x x}]}{\left(\frac{\omega_{\mathrm{wk}_x}}{c}\right)^2 \cdot \mathcal{E}_y^{(e)\mathrm{wk}_x}(x)e^{ik_x x}}. \quad \text{(A6)}$$

The absolute value of $\mathcal{W}_G^{(e)\mathrm{wk}_x}$ (calculated for the same PhC parameters used in the main text) is shown in panel (a) of Fig. 7 while the results of the reconstruction of the lowest-frequency even mode ($\mathrm{M}_0^{(e)}$) of the L_{11} cavity are summarized in the lower part of the figure. The reconstructed field distribution of the mode is in very good agreement with the one computed with the 2DFD method. This confirms the possibility of treating the even modes of L_N-like PhC cavities within the formalism introduced in Sec. II, further attesting to the general validity of our approach.

*marco.felici@epfl.ch

[1] D. E. Aspnes, Surf. Sci. **132**, 406 (1983).
[2] F. Capasso, Science **235**, 172 (1987).
[3] *Dilute Nitride Semiconductors*, edited by M. Henini (Elsevier, Oxford, UK, 2005).
[4] K. Yu, W. Walukiewicz, J. Wu, D. Mars, D. Chamberlin, M. Scarpulla, O. Dubon, and J. Geisz, Nature Mater. **1**, 185 (2002).
[5] K. M. Yu, W. Walukiewicz, J. Wu, W. Shan, J. W. Beeman, M. A. Scarpulla, O. D. Dubon, and P. Becla, Phys. Rev. Lett. **91**, 246403 (2003).
[6] M. Felici, A. Polimeni, G. Salviati, L. Lazzarini, N. Armani, F. Masia, M. Capizzi, F. Martelli, M. Lazzarino, G. Bais, M. Piccin, S. Rubini, and A. Franciosi, Adv. Mater. **18**, 1993 (2006).
[7] G. Allison, S. Spasov, A. Patane, L. Eaves, A. Ignatov, D. K. Maude, M. Hopkinson, and R. Airey, Phys. Rev. B **75**, 115325 (2007).
[8] G. Pettinari, A. Polimeni, F. Masia, R. Trotta, M. Felici, M. Capizzi, T. Niebling, W. Stolz, and P. J. Klar, Phys. Rev. Lett. **98**, 146402 (2007).
[9] P. Y. Yu and M. Cardona, *Fundamentals of Semiconductors-Physics and Materials Properties* (Springer-Verlag, Berlin, Germany, 1996).
[10] S. John, Phys. Rev. Lett. **58**, 2486 (1987).
[11] E. Yablonovitch, Phys. Rev. Lett. **58**, 2059 (1987).
[12] J. Foresi, P. Villeneuve, J. Ferrera, E. Thoen, G. Steinmeyer, S. Fan, J. Joannopoulos, L. Kimerling, H. Smith, and E. Ippen, Nature (London) **390**, 143 (1997).
[13] T. Baba, N. Fukaya, and J. Yonekura, Electron. Lett. **35**, 654 (1999).
[14] O. Painter, R. K. Lee, A. Scherer, A. Yariv, J. D. O'Brien, P. D. Dapkus, and I. Kim, Science **284**, 1819 (1999).
[15] S. Strauf, K. Hennessy, M. T. Rakher, Y. S. Choi, A. Badolato, L. C. Andreani, E. L. Hu, P. M. Petroff, and D. Bouwmeester, Phys. Rev. Lett. **96**, 127404 (2006).
[16] T. Yoshie, A. Scherer, J. Hendrickson, G. Khitrova, H. M. Gibbs, G. Rupper, C. Ell, O. B. Shchekin, and D. G. Deppe, Nature (London) **432**, 200 (2004).
[17] K. Hennessy, A. Badolato, M. Winger, D. Gerace, M. Atatüre, S. Gulde, S. Fält, E. Hu, and A. Imamoğlu, Nature (London) **445**, 896 (2007).
[18] G. Khitrova, H. M. Gibbs, M. Kira, S. W. Koch, and A. Scherer, Nat. Phys. **2**, 81 (2006).

[19] Y. Akahane, T. Asano, B. Song, and S. Noda, Appl. Phys. Lett. **83**, 1512 (2003).
[20] P. Gallo, M. Felici, B. Dwir, K. A. Atlasov, K. F. Karlsson, A. Rudra, A. Mohan, G. Biasiol, L. Sorba, and E. Kapon, Appl. Phys. Lett. **92**, 263101 (2008).
[21] Y. Akahane, T. Asano, B. S. Song, and S. Noda, Nature (London) **425**, 944 (2003).
[22] Y. Akahane, T. Asano, B. Song, and S. Noda, Opt. Express **13**, 1202 (2005).
[23] B. Song, S. Noda, T. Asano, and Y. Akahane, Nature Mater. **4**, 207 (2005).
[24] J. D. Joannopoulos, R. D. Meade, and J. N. Winn, *Photonic Crystals: Molding the Flow of Light* (Princeton University Press, Princeton, 1995).
[25] M. Qiu, Appl. Phys. Lett. **81**, 1163 (2002).
[26] A. Taflove and S. C. Hagness, *Computational Electrodynamics: The Finite-Difference Time-Domain Method* (Artech, Norwood, MA, 2000).
[27] M. Felici, P. Gallo, A. Mohan, B. Dwir, A. Rudra, and E. Kapon, Small **5**, 938 (2009).
[28] K. A. Atlasov, K. Karlsson, E. Deichsel, A. Rudra, B. Dwir, and E. Kapon, Appl. Phys. Lett. **90**, 153107 (2007).
[29] D. T. F. Marple, J. Appl. Phys. **35**, 1241 (1964).
[30] K. Sakoda, *Optical Properties of Photonic Crystals* (Springer-Verlag, Berlin, Germany, 2005).
[31] K. A. Atlasov, M. Felici, K. F. Karlsson, P. Gallo, A. Rudra, B. Dwir, and E. Kapon, Opt. Express **18**, 117 (2010).
[32] V. S. C. Manga Rao and S. Hughes, Phys. Rev. Lett. **99**, 193901 (2007).
[33] D. Englund, I. Fushman, and J. Vuckovic, Opt. Express **13**, 5961 (2005).
[34] J. Vučković, M. Loncar, H. Mabuchi, and A. Scherer, Phys. Rev. E **65**, 016608 (2001).
[35] K. Srinivasan and O. Painter, Opt. Express **10**, 670 (2002).
[36] K. Srinivasan and O. Painter, Opt. Express **11**, 579 (2003).
[37] J. M. Geremia, J. B. Williams, and H. Mabuchi, Phys. Rev. E **66**, 066606 (2002).
[38] For instance, the minimum pixel size of the Vistec EBPG5000 lithography system available in our department is 1.25 nm. For an example of the results attainable with this system, see Ref. 39.
[39] A. Surrente, P. Gallo, M. Felici, B. Dwir, A. Rudra, and E. Kapon, Nanotechnology **20**, 415205 (2009).
[40] A. F. Oskooi, D. Roundy, M. Ibanescu, P. Bermel, J. D. Joannopoulos, and S. G. Johnson, Comput. Phys. Commun. **181**, 687 (2010).
[41] V. Mandelshtam and H. Taylor, J. Chem. Phys. **107**, 6756 (1997).
[42] V. Mandelshtam and H. Taylor, J. Chem. Phys. **109**, 4128 (1998).
[43] Such a structure would be interesting for the realization of PhC microcavity lasers based on a series of site-controlled QDs, coupled to the equally intense antinodes of the designed cavity mode.
[44] S. V. Zhukovsky, D. N. Chigrin, A. V. Lavrinenko, and J. Kroha, Phys. Rev. Lett. **99**, 073902 (2007).
[45] K. A. Atlasov, K. F. Karlsson, A. Rudra, B. Dwir, and E. Kapon, Opt. Express **16**, 16255 (2008).
[46] D. Englund, A. Faraon, B. Zhang, Y. Yamamoto, and J. Vuckovic, Opt. Express **15**, 5550 (2007).
[47] A. Mohan, M. Felici, P. Gallo, B. Dwir, A. Rudra, J. Faist, and E. Kapon, Nat. Photonics **4**, 302 (2010).